Photophysics of a Live-Cell-Marker, Red Silicon-Substituted Xanthene Dye.

*Luis Crovetto,[1] Angel Orte,[1] Jose M. Paredes,[1] Sandra Resa,[2] Javier Valverde,[1] Fabio Castello,[1] Delia Miguel,[2] Juan M. Cuerva,[2] Eva M. Talavera,[1] and Jose M. Alvarez-Pez[1,]**

[1] Department of Physical Chemistry, Faculty of Pharmacy, University of Granada, Cartuja Campus, 18071 Granada, Spain.

[2] Department of Organic Chemistry, Faculty of Sciences, University of Granada, C. U. Fuentenueva s/n, 18071 Granada, Spain.

ABSTRACT. Dyes with near-red emission are of great interest because of their undoubted advantages for use as probes in living cells. In-depth knowledge of their photophysics is essential for employment of such dyes. In this article, the photophysical behavior of a new silicon-substituted xanthene, 7-hydroxy-5,5-dimethyl-10-(o-tolyl)dibenzo[b,e]silin-3(5H)-one (**2-Me TM**), was explored using absorption, steady-state, and time-resolved fluorescence. First, the near-neutral pH, ground state acidity constant of the dye, $pK^*_{N\text{-}A}$, was determined by both absorbance and steady-state fluorescence methods in the presence of very low buffer concentrations. Next, we determined whether the addition of phosphate buffer promoted the excited-state proton exchange reaction between the neutral and anion form of **2-Me TM** in aqueous solutions at near-neutral pH. For this analysis, both the steady-state fluorescence method and time-resolved emission spectroscopy (TRES) were employed. The TRES experiments demonstrated a remarkably favored conversion of the neutral form to the anion form. Then, fluorescence decay traces recorded as a function of buffer concentration and pH were globally analyzed to determine the values of the excited-state rate constants. The revealed kinetic parameters were consistent with the TRES results, exhibiting a higher rate constant for deprotonation than for protonation, which implies an unusual low value of the excited-state acidity constant $pK^*_{N\text{-}A}$ and therefore an enhanced photoacid behavior of the neutral form. Finally, we determined whether **2-Me TM** could be used as a sensor inside live cells by measuring the intensity profile of the probe in different cellular compartments of HeLa 229 cells.

1. Introduction

The family of fluorescein derivatives has been widely employed for use as fluorescent probes because of their high water solubility and favorable spectral parameters, including the high molar extinction coefficient of the dianion form at a wavelength of 490 nm, which matches the 488 nm spectral line of the argon ion laser, and their high fluorescence quantum yield.[1-2] Although fluorescein in aqueous solution can exist in four different prototropic forms, depending on the pH, at near-neutral pH values, only the dianion and monoanion forms, with different absorption spectra and fluorescence quantum yields, are important.[3] Because of the spectral changes associated with the monoanion-dianion transition, fluorescein has been employed as a pH probe, although the BCECF derivative [2',7'-bis-(2-carboxyethyl)-5-(and-6)-carboxyfluorescein][4-5] is preferred for measuring pH values in biological systems because it has the additional advantage that its ground-state acidity constant corresponds to a near-neutral pH.[6]

Various fluorescein derivatives, in which methyl, methoxy, or *tert*-butyl groups have been introduced into the benzene moiety, have been synthesized in the last decade.[7-8] These dyes have the additional advantage of providing a single anion species in aqueous solution, and some behave as on/off fluorescent probes. Among the latter, 9-[1-(2-methyl-4-methoxyphenyl)]-6-hydroxy-3H-xanthen-3-one (**2-Me-4-OMe TG**) and 9-[1-(4-tert-butyl-2-methoxyphenyl)]-6-hydroxy-3H-xanthen-3-one (Granada Green, **GG**), which both emit green fluorescence, have been used as fluorescent indicators of phosphate ions in living cells in fluorescence lifetime imaging microscopy (FLIM).[9-10] Although the FLIM methodology is adequate for removing the contribution of the auto-fluorescence of cells and biological fluids, it is also interesting to explore dyes that emit in other color regions for their use in bioimaging. Since the first red-emission silaanthracene fluorophore (TMDHS) was synthesized by Fu *et al.*,[11] fluorescent probes

both silicon-substituted rhodamines,[12-13] and silicon-substituted fluoresceins,[14-16] have been synthesized and developed as labeling and bioimaging reagents. The interested reader can be directed to a topical minireview covering recent progress on silicon-substituted xanthene dyes.[17] In this context, one significant dye silicon-substituted xanthene, the 7-hydroxy-5,5-dimethyl-10-(o-tolyl)dibenzo[b,e]silin-3(5H)-one (**2-Me TM**)[18] was recently synthesized. This dye exhibits absorption and emission wavelengths that are approximately 90 nm longer than those of fluorescein derivatives.

As it is recognized, the use of fluorescent probes as these silicon-substituted xanthene derivatives as sensors, requires a full understanding of the complex photophysics of the dyes. It has been well established that fluorescein derivatives have the ability to undergo excited-state proton transfer reactions (ESPT), thereby rapidly interconverting between two protonated forms in the presence of a suitable proton donor-acceptor. For instance, the ionic species of phosphate buffer act as a suitable proton donor-acceptor to promote ESPT in fluorescein[2] or BCECF,[6] whereas a lower-pK_a buffer, such as acetate buffer, promotes ESPT reactions in 2',7'-difluorofluorescein (Oregon Green 488, **OG488**).[19-20] To fully understand the complex photophysics of these new silicon-substituted xanthene derivatives, one must focus on the excited-state dynamics of the molecular forms present at near physiological pH values because the presence of the excited-state reactions influences the fluorescent decay from excited prototropic forms, exhibiting complex kinetics and different decay times that depend on both the pH and buffer concentration. Nevertheless, the presence of ESPT reactions could be advantageous because in these reactions, the decay times are tuned by the phosphate buffer concentration at a determined pH, thus sensing the phosphate concentration of either a complex solution or living cells.[9-10]

The time-correlated single-photon counting (TCSPC)[21] technique supplies fluorescence data from which both the time-resolved emission spectra (TRES) and other relevant photophysical parameters of the system can be obtained. TRES are fluorescence spectra obtained at discrete times in the course of the fluorescence decay. To perform TRES and determine the appropriate relaxation model to describe the photophysical system, a tridimensional fluorescence decay surface that represents the fluorescence intensity at all wavelengths and times during the fluorescence decay is measured. Thus, the reconstructed emission is defined in terms of both the spectral and time resolution.[22] Once it is demonstrated that the spectra family corresponds to a system in two excited states, a suitable model of ESPT in the presence of a proton donor/acceptor should be proposed to determine the significant photophysical parameters.[2] To resolve the model, a multidimensional fluorescence decay data surface under various experimental conditions, specifically with respect to the excitation (λ_{ex}) and emission (λ_{em}) wavelengths, pH, and buffer concentration, C^B, is measured. Finally, to achieve an accurate estimation of the parameters, the fluorescence decay traces should be analyzed in terms of their decay times (τ_i) and associated amplitudes (p_i) by the global analysis approach, in which the τ_i values can be determined from decay traces for the same sample collected at various excitation and emission wavelengths.[23] A full study of the variation of the decay times with pH and buffer concentration enables determination of the underlying rate constants (k_{ij}) that define the excited-state kinetics.[24] Using these rate constant values, the steady-state fluorescence intensity and fluorescence decay time values may be calculated at any pH and proton donor/acceptor concentration.[2, 20]

In this paper, aqueous solutions of **2-Me TM** were investigated via absorption, steady-state and time-resolved emission spectroscopy. The ground-state equilibrium between the neutral and

anionic forms of **2-Me TM** was examined, and the acidity constant was measured through absorption and fluorometric titrations. Next, both steady-state and TRES methodologies were employed to reveal the buffer-mediated two-excited-state photophysics system. Finally, the pertinent kinetic ESPT reaction model and its dynamics were studied in detail using time-resolved fluorescence measurements. The underlying kinetic rate constants, which describe the dynamic behavior of the system, were determined via global analysis of the multi-dimensional fluorescence decay surface collected as a function of λ_{ex}, λ_{em}, pH, and C^B. Finally, the applicability of **2-Me TM** for bioimaging was determined using HeLa 229 cells by collecting the emitted near-red signal with a fluorescence microscope system.

2. Experimental Methods

2.1. Materials and Preparation of Solutions

For the preparation of phosphate buffer solutions, $NaH_2PO_4 \cdot H_2O$ and $Na_2HPO_4 \cdot 7H_2O$ (both Fluka, puriss. p.a.) were used. Solutions of NaOH and $HClO_4$ (0.01 M) were used to adjust the pH of the aqueous solutions (without buffer). NaOH (platelets, Sigma-Aldrich, Spain) and $HClO_4$ (Sigma-Aldrich) were of spectroscopic grade. All of the solutions were prepared using Milli-Q water as a solvent. All of the chemicals were used as received without further purification.

2-Me TM was synthesized with a good yield (85%) by the addition of commercially available *o*-tolylmagnesium bromide to 3,7-bis((tert-butyldimethylsilyl)oxy)-5,5-dimethyldibenzo[b,e]silin-10(5H)-one **I** and subsequent dehydration with aqueous hydrochloric acid (Scheme 1). The corresponding TBDMS-derivative **I** was prepared following the protocol

described by Best *et al*.[25] The purity of **2-Me TM** was confirmed by ^{1}H-NMR, and ^{13}C-NMR (data and figures in the SI).

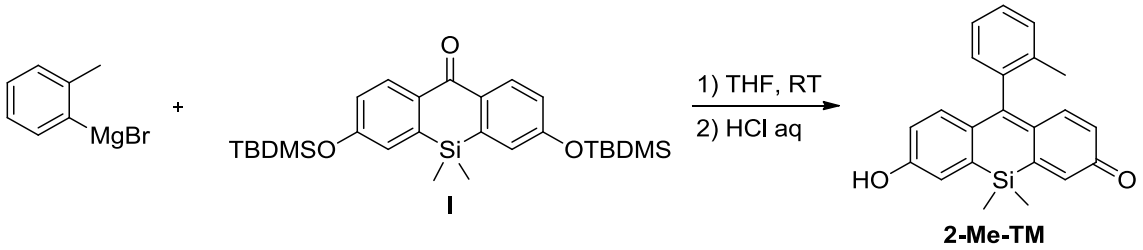

Scheme 1. Synthesis of the **2-Me TM** derivative.

A stock solution of **2-Me TM** (10^{-4} M) in 10^{-3} M NaOH was prepared using Milli-Q water. Using this stock solution, the required concentrations of **2-Me TM** in the appropriate concentrations of NaH_2PO_4 or Na_2HPO_4 solutions were prepared. The required volumes of these solutions were then mixed to obtain the pH values used in the experiments. For fluorescence measurements, non-degassed solutions were prepared such that the absorbance of the final solutions at λ_{ex} was less than 0.1. The solutions were kept cool in the dark when not in use to avoid possible deterioration through exposure to light and heat.

For the pK_a calculation using the absorbance or steady-state fluorescence experiments, eleven solutions of **2-Me TM** (5×10^{-5} M or 5×10^{-6} M, respectively) in 0.05 M phosphate buffer with pH values in the range of 6.18 to 10.14 were prepared. For the TRES experiments, eight solutions of **2-Me TM** (5×10^{-6} M) in 0.7 M phosphate buffer with pH values in the range of 3.97 to 8.72 were prepared, and each solution was excited at either 485 or 530 nm to preferentially excite the neutral or anion form. The decay traces from each solution at each excitation wavelength were registered at each 5 nm in the emission wavelength range from 550 to 640 nm. To construct the multi-dimensional fluorescence decay surface to determine the fundamental kinetic parameters, eleven solutions without buffer were prepared within a pH range of 4.0-9.5

and in the presence of phosphate buffer (C^B = 0.05, 0.15, 0.30 and 0.6 M); forty-four solutions were prepared within a pH range of 4.0-9.5.

The HeLa 229 (ECACC 86090201) cell line was provided by the Cell Culture Facility, University of Granada. The cells were grown in Dulbecco's Modified Eagle's medium (DMEM) supplemented with 10% (v/v) FBS, 2 mM glutamine, 100 U/ml penicillin, and 0.1 µg/ml streptomycin in a humidified 5% CO_2 incubator. For the fluorescence imaging microscopy experiments, HeLa 229 cells were seeded onto 20-mm diameter coverslips in 6-well plates. The coverslips were transferred to the MicroTime 200 fluorescence microscope system (see below) and washed with Krebs-Ringer-Phosphate (KRP) buffer before addition of the working solutions. The KRP buffer was prepared at pH 7.4 and contained the following: NaCl 118 mM, KCl 5 mM, $CaCl_2$ 1.3 mM, $MgCl_2$ 1.2 mM, KH_2PO_4 1.2 mM and Hepes 30 mM (all chemicals from Sigma-Aldrich). The working solutions were prepared using KRP buffer and **2-Me TM** (10^{-7} M).

2.2. Instrumentation

Absorption spectra were recorded using a Perkin-Elmer Lambda 650 UV/Vis spectrophotometer with a Peltier temperature controller. Steady-state fluorescence emission spectra were collected using a JASCO FP-6500 spectrofluorometer equipped with a 450-W xenon lamp for excitation with an ETC-273T temperature controller. All measurements were recorded at 20 ºC using 10 × 10 mm cuvettes. The pH of the solutions was measured immediately after recording each spectrum.

Fluorescence decay traces were recorded via the time-correlated single photon counting (TCSPC)[21, 26] method using a FluoTime 200 fluorometer (PicoQuant GmbH, Germany). The excitation source consisted of either an LDH-485 or LDH-530 pulsed laser (PicoQuant) with a

minimum pulse width of 88 ps. The pulse repetition rate was 20 MHz. The laser pulse was directed to the solution sample in the 10×10 mm cuvettes. The lens-focused fluorescence emission passed through a detection polarizer set at the magic angle and a detection monochromator prior to detection by the photomultiplier detector. The fluorescence decay histograms were collected in 1,320 channels with a time increment of 36 ps/channel. Histograms of the instrument response functions (using the LUDOX scatter) and sample decays were recorded until they reached 2×10^4 counts on the peak channel. In the TRES experiments, when the count rate was very low in the extreme portion of the emission wavelength range chosen (550 to 640 nm), the decay traces were collected for five minutes to achieve a count number sufficient for analysis.

Fluorescence imaging microscopy was performed on a MicroTime 200 fluorescence microscope system (PicoQuant). The excitation source consisted of the LDH-530 pulsed laser described previously. The light beam was directed onto a dichroic mirror (Z532RDC, Chroma) and to the oil immersion objective (1.4 NA, 100×) of an inverted microscope system (IX-71, Olympus). The collected fluorescence light was filtered by a long-pass filter (550LP, AHF/Chroma) and focused onto a 75-μm confocal aperture. After passing through the aperture, the transmitted light passed through an FB600-40 bandpass filter (Thorlabs) and was refocused onto single-photon avalanche diodes (SPCM-AQR 14, Perkin Elmer). The data acquisition was performed with a TimeHarp 200 TCSPC module (PicoQuant). Raw images were recorded via raster scanning with a resolution of 512 × 512 pixels. The fluorescence images were analyzed using Fiji ([Fiji Is Just] ImageJ), an open-source platform for biological-image analysis.[27]

2.3. Fluorescence decay trace analysis

The fluorescence decay traces for TRES were individually analyzed using an iterative deconvolution method with exponential models using the FluoFit software package (PicoQuant). The impulse response curves, either collected with the same number of counts at the peak or in a discrete period of time when the emission intensity was low, were corrected and then normalized to a steady-state emission spectrum recorded on the same instrument.

The decay traces of solutions at the same pH, buffer concentration, and excitation wavelength were globally analyzed using the FluoFit software package. The decay times were linked as shared parameters, whereas the pre-exponential factors were considered local adjustable parameters.

3. Results and Discussion

*3.1. Absorption measurements and ground-state equilibria of **2-Me TM***

The visible absorption spectra of aqueous solutions of **2-Me TM** (5×10^{-5} M) in a pH range between –0.40 and 10.14 were recorded at very low ionic strength (0.01 M phosphate buffer). The absorption spectra of solutions at different pH values exhibited pH-induced transitions due to ground-state proton reactions, which were dictated by the ground-state pK_a values. In Figure 1A, two different isosbestic points can be distinguished: one occurs at approximately 505 nm with moderate acid or basic pH values, and the other, at low pH values, occurs at 485 nm. The similarity of the chemical structure of **2-Me TM** to those of 2-OMe-5-Me TG and 2-Me-4-OMe TG[28-29] and the number of isosbestic points suggest that **2-Me TM** in aqueous solution presents three visible absorbing protonated forms, the cation (C), neutral (N), and anion (A) forms, and two ground-state pK_a involved in the acid-base transitions (Scheme 2). The N and A forms are the only relevant species at near-neutral pH values.

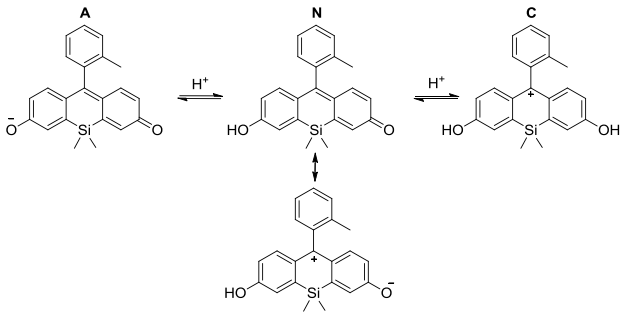

Scheme 2. Prototropic forms of **2-Me TM**, **A** (anion), **N** (neutral) and **C** (cation). Neutral form is represented by two resonance structures.

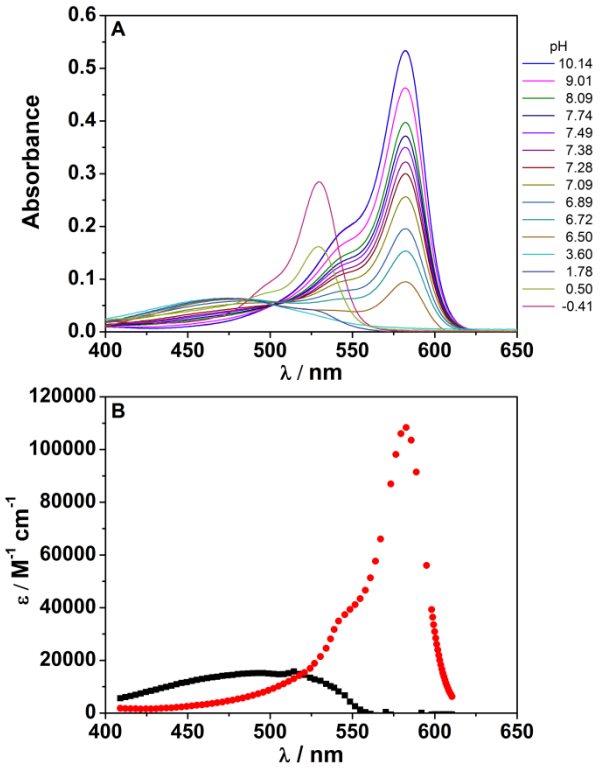

Figure 1. A) Absorption spectra of aqueous solutions of **2-Me TM** (5×10^{-6} M) at pH values between –0.4 and 10.14. B) Recovered molar absorption coefficients versus wavelength for the neutral (black) and anionic (red) form of **2-Me TM**.

As shown in Figure 1A, at a basic pH, the spectrum is essentially composed of a band centered at 585 nm and a shoulder at approximately 550 nm, which is identical to the spectrum observed in NaOH (1 M). With decreasing pH, the shoulder disappears, the band that peaks at 585 nm is blue-shifted and its absorbance decreases, and the profile of the absorption band is very broad, exhibiting a small pronounced maximum. At a pH of approximately 4.00, the spectrum shape is a wide band with a diffuse maximum at approximately 475 nm. The absorption spectra at pH values ranging between 6.50 and 10.14 exhibit only one transition at near-neutral pH, which is characterized by the ground-state constant $K_{N\text{-}A}$. The recovered spectra in this pH range, and their appointment of them to both anion and neutral prototropic forms, are concordant with those recently reported.[15] At pH values of less than 6.50, in the pH range –0.4 to 3.60, a wide band with a diffuse maximum at approximately 475 nm was red-shifted as a new band arises, peaking at 530 nm. In that pH range, another isosbestic point at 485 nm can be clearly distinguished, thus indicating that another species is involved in this other acid-base equilibrium, characterized by the ground-state constant $K_{C\text{-}N}$. The absorption spectrum of the cation form was confirmed using a 2.0 M $HClO_4$ aqueous solution, and it exhibited a peak at 530 nm. Thus, the experimental visible absorption spectra of **2-Me TM** aqueous solutions in the pH range between –0.4 and 10.14 is consistent with the ionic equilibria between the prototopic forms depicted in Scheme 2.

The absorbance (A) of the aqueous solutions of **2-Me TM** depends on the pH according to the acid-base equilibrium theory and Beer's law. Because the only pK_a of interest for biological applications is that which the dye presents at near–neutral pH, the selected absorption spectra at pH values ranging between 6.50 and 10.14 were analyzed. The nonlinear global fitting of the entire surface of A vs. pH vs. λ_{abs} to Beer's law and the corresponding acid-base equilibrium

equations (see SI eq. S1 to S3) enables determination of the molar absorption coefficients $\varepsilon_i(\lambda_{abs})$ and pK_{N-A}.[3] In the global fitting, the pK_{N-A} was a linked parameter over the entire surface, whereas $\varepsilon_i(\lambda_{abs})$ was a locally adjustable parameter at each wavelength for each species. The absorbance data surface was composed of 11 pH values and 224 λ_{abs} values between 400 and 624 nm at each pH. Beer's law for two protonated species provided the best fit to the experimental absorption data. Plots of the individual *A vs*. pH curves at different wavelengths and the curves generated from the fitting are shown in Figure S3 (SI). In the data surface fitting process, the estimated parameter values were independent of the initial guesses assigned to these parameters. Figure 1B shows the recovered values of the molar absorption coefficients of the neutral (ε_N) and anionic forms (ε_A) in 0.01 M phosphate buffer. The observed pK_{N-A} value was 7.31 ± 0.03.

3.2. Steady-state emission spectra

In Figure 2, the three different emission spectral profiles that correspond to the three prototropic forms are shown. In contrast with other xanthene dye, the cation exhibited no photoacid behavior (see Figure S4).[20, 29] Nevertheless, the spectral profile of the cation form shown in Figure 2 was recorded in a 2.0-M $HClO_4$ aqueous solution.

The ground state acid-base equilibrium constants can also be obtained by fluorometric titrations whenever there is constant intensity of excitation, low absorbance values, and negligible rates of proton transfer in the excited state. Therefore, the steady-state fluorescence spectra of **2-Me TM** solutions in the pH range from 6.18 to 9.00 were recorded at two excitation wavelengths (485 and 580 nm). To minimize the rate of possible ESPT reactions mediated by the presence of a proton donor/acceptor, we used phosphate (0.005 M) as a buffer.[30] Only the A and

N emission spectral profiles were detected in that pH range. The acidity constant (pK_a) value between the neutral and anion forms of **2-Me TM** was 7.41 ± 0.02. Representative examples of the emission spectra and fits to the experimental data are shown in Figures S5 and S6 in the SI.

The pK_a values from the absorbance and emission measurements were consistent and slightly greater than the previously reported value of 6.8, although this latest value was determined in the presence of phosphate buffer (0.1 M) and 1% dimethyl sulfoxide (DMSO).[18]

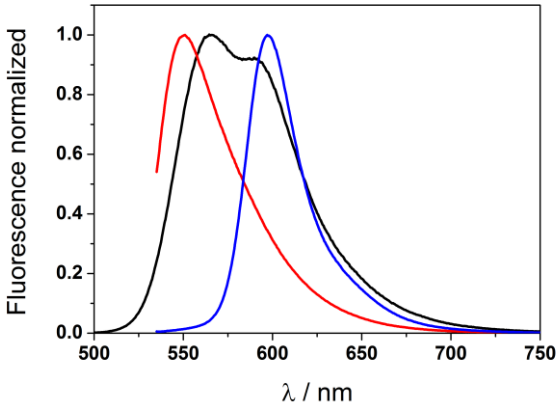

Figure 2. Normalized fluorescence spectral profiles of the three prototropic forms of **2-Me TM**: anion (blue), neutral (black), and cation (red).

3.3. Buffer-Mediated ESPT Reactions

Xanthene derivatives undergo fast proton transfer reactions in the excited-state when a suitable proton donor/acceptor is present in solution at an adequate concentration. The occurrence of these reactions may dramatically change the outcome of steady-state or time-resolved fluorescence experiments if it is not taken into account. **2-Me TM** can undergo such reactions when mediated by the presence of the prototropic forms of the phosphate buffer, and we explore these reactions here.

The steady-state fluorescence spectra from aqueous 5×10^{-6} M solutions of **2-Me TM** at pH 6.10 in the presence of different concentrations of phosphate buffer in the range of 0.010-0.75 M were recorded from 500 to 700 nm using an excitation wavelength of 485 nm. The observed spectra are shown in Figure 3. This figure shows that with these experimental conditions, an increase in the buffer concentration resulted in both a pronounced redshift and an increasing intensity of the emission band, which peaked at 600 nm. Moreover, a concomitant decrease in the emission band that peaks at 560 nm, which is attributable to the neutral species, was also observed. The above results are indicative of an ESPT reaction promoted by the phosphate buffer. Indeed, both the 485-nm excitation wavelength and with the pH of 6.10 preferentially excite the much-less-fluorescent **2-Me TM** neutral form. Then, the buffer-mediated ESPT reaction rapidly occurred during the lifetime of the two excited-state system, thus forming the much more fluorescent anion form and causing variation in the spectral profile and fluorescence intensity.

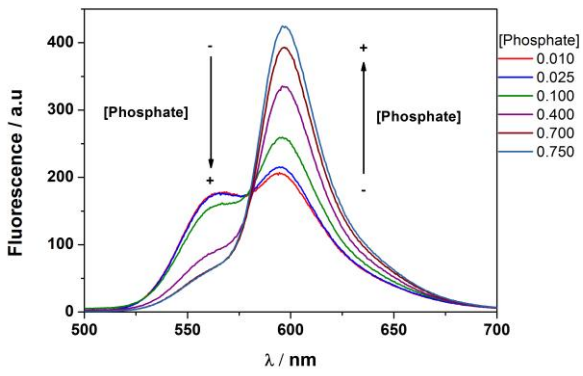

Figure 3. Steady-state emission spectra from 5×10^{-6} M **2-Me TM** aqueous solutions at a pH of 6.10 and different phosphate buffer concentrations ranging from 0.010 to 0.75 M (λ_{ex}= 485 nm).

To observe the dynamic properties of the fluorescent emission, we also collected the fluorescence decay traces from the same solutions employed in the previous experiment. The excitation wavelength was 485 nm, and the emission wavelength was 610 nm, which preferentially detects the anionic species. The results are shown in Figure S7, in which only 4 decay traces are shown for clarity. It is apparent from the figure that increasing the phosphate concentration caused an increase in the fluorescence decay time. This result is consistent with the idea that the neutral species (which was excited preferentially in this experiment) undergoes an ESPT reaction during the lifetime of the excited state, which is influenced by the concentration of phosphate buffer. In the ESPT reaction, a portion of the excited neutral species becomes an excited anion, and if the reaction occurs sufficiently quickly, both species decay simultaneously. As previously mentioned, the reaction rate depends on the phosphate concentration; therefore, at a higher buffer concentration, the reaction will be faster, and the corresponding amount of the anion, which is dictated by the $pK^*_{N\text{-}A}$ and pH of the experiment, will be formed earlier. Thus, the subsequent fluorescence decay corresponds to the two coupled species. If the neutral/anion relationship corresponding to the pH of the experiment is achieved faster, the coupled fluorescence of the system will be detected for longer times.

3.4. TRES

The ESPT reaction mediated by phosphate should exhibit a double-exponential decay behavior, with decay times independent of the wavelength of emission but dependent on the forward and reverse rates of the ESPT reaction.[2] Therefore, the fluorescence spectra observed at discrete times during the fluorescence decay (TRES) can provide detailed information about the photophysical two-excited-state system. To accomplish this goal, we performed TRES with

decay traces collected from aqueous solutions of **2-Me TM** in 0.7 M phosphate buffer and at eight pH values in the range 4.00 to 8.70, and using the excitation wavelengths of 485 and 530 nm to preferentially excite either the neutral or the anionic species, respectively. Emission in the wavelength range of 550-640 nm was recorded in 5 nm steps. The complete data matrix is composed of 304 decay traces and can be described by a three-dimensional surface, $I(\lambda_{ex}, \lambda_{em}, t)$, that represents the fluorescence intensity at all excitation and emission wavelengths and times during the fluorescence decay. All of the decay traces could be adjusted using biexponential functions. It should be mentioned that for the emission wavelengths corresponding to the ends of the experimental range, the decay traces had low fluorescent signals. Therefore, the decay traces were recorded for different collection times, and hence the pre-exponential coefficients at each wavelength were corrected by the collection time and then normalized to the same count number in the decay. Thus, the decay traces were proportional to the steady-state fluorescence intensity. The pre-exponential factors were also corrected for the different sensitivity of the detector using a factor that related the total emission during the decay ($p_1 \times \tau_1 + p_2 \times \tau_2$) to the steady-state-intensity emission.

Figure 4 shows the TRES generated at pH 5.90 and both λ_{ex} = 485 and 530 nm. The TRES are represented by a plot of the fluorescence intensity level as a function of time and emission wavelength (Fig. 4A and C), along with the normalized emission spectra at different times after the excitation pulse in the range of 0-4 ns (Fig. 4B and D).

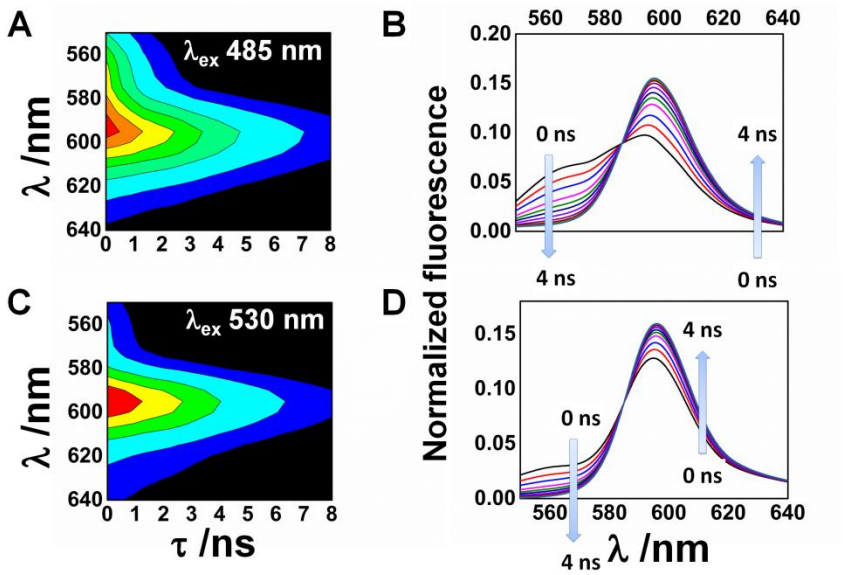

Figure 4. Contours of fluorescence intensity of **2-Me TM** after a δ-pulse excitation as a function of time and λ_{em} in 0.7 M phosphate buffer at pH 5.90 (A: λ_{ex} 485 nm; C: λ_{ex} 530 nm). The corresponding normalized emission spectra at different times after the excitation pulse are shown (B: λ_{ex} 485 nm; D: λ_{ex} 530 nm).

The spectrum profile at a shorter time after the pulse in Figure 4B reflects a large amount of the neutral species, which was preferentially excited under the experimental conditions employed (λ_{ex} = 485 mm). With increasing emission time, the spectral profile was gradually red-shifted, thus reflecting the successive greater abundance of the anionic species. Finally, after a longer time, the profile remained virtually unchanged because the neutral/anion relationship dictated by the pK_a* and pH of the experiment was achieved. When the anion species was preferentially excited at a wavelength of 530 nm (and the same pH of 5.90), the initial spectral profile exhibited a small contribution of the neutral species. Remarkably, the spectral profiles also

reflect a successive greater abundance in the anionic species with increasing emission time (Figure 4D), thereby demonstrating that the p$K^*_{N\text{-}A}$ of the excited state is significantly less than the pH of the experiment. Different fluorescent spectral shapes were obtained by determining the spectra at each excitation wavelength using several pH values. In the SI (Figures S8 and S9), different illustrative examples of plots of fluorescence intensity versus time and emission wavelength, along with the normalized emission spectra at different times of emission, are shown. In brief, the spectral profiles were consistent with the phosphate-mediated ESPT reaction between the neutral and anionic species of **2-Me TM**. Moreover, the TRES experiments demonstrated a preferred conversion of the neutral form (defined by the shoulder at 560 nm) to the anion form (which exhibited an emission maximum at 590 nm). This finding indicates that buffer-mediated deprotonation of the neutral form is the main process, whereas buffer-mediated protonation of the anion form is a much slower process.

3.5. Kinetic and spectral parameters of the phosphate-mediated ESPT reaction

Once experimental evidence of the photophysical two-excited-state system was obtained, a multi-dimensional fluorescence decay surface was used to determine the kinetic parameters and gain insights into the kinetic behavior of the system in the excited state. Scheme 3 shows the reactions involved in the ESPT and the fluorescence emission for the two species of **2-Me TM** present at near-neutral pH.

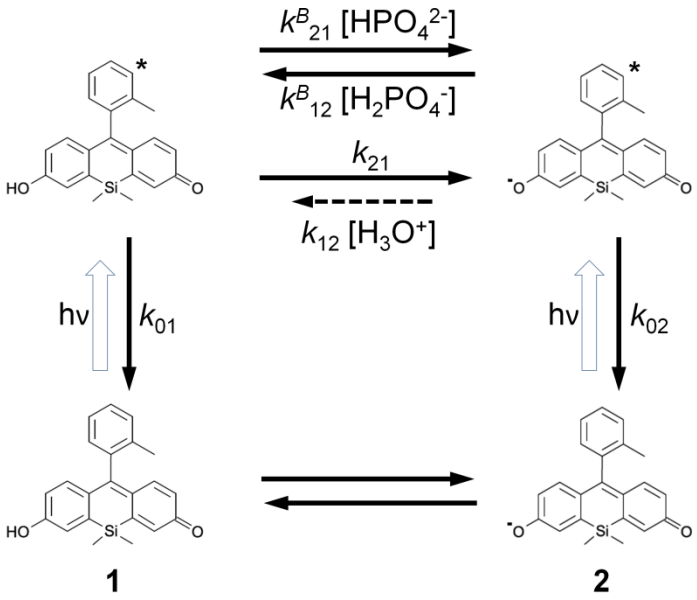

Scheme 3. Kinetic model of ground- and excited-state proton-exchange reactions of **2-Me TM** in the presence of a phosphate buffer.

In Scheme 3, species **1** and **2** are the neutral and anionic forms of **2-Me TM**, respectively. Following excitation by a fast δ-pulse of light, the excited-state species, $\mathbf{1}^*$ and $\mathbf{2}^*$ are created. These excited species can decay through fluorescence (F) and non-radiative (NR) processes. The composite rate constants for these processes are denoted by k_{01} (= k_{F1} + k_{NR1}) and k_{02} (= k_{F2} + k_{NR2}). k_{21} denotes the rate constant for the dissociation of $\mathbf{1}^*$ into $\mathbf{2}^*$ and H^+. Because in the experimental pH range, [H^+] is sufficiently small, the rate of association of $\mathbf{2}^* + H^+ \rightarrow \mathbf{1}^*$ (k_{12}) can be considered negligible. The ground-state proton exchange reaction of **2-Me TM** is described by the acidity constant $K_{\text{N-A}}$. The acidity constant of the buffer is denoted by K_a^B = [HPO_4^{2-}][H^+]/[$H_2PO_4^-$]. In the excited state, the reaction of $\mathbf{1}^*$ with HPO_4^{2-} to form $\mathbf{2}^*$ and

$H_2PO_4^-$ is characterized by the rate constant k_{21}^B. The reverse reaction of $\mathbf{2}^*$ and $H_2PO_4^-$ that yields $\mathbf{1}^*$ and HPO_4^{2-} is described by the rate constant k_{12}^B.

The theory and methods of solving buffer-mediated ESPT reactions are well-established[2, 20, 24, 31] (see also the SI). To achieve a unique determination of the rate constants, fluorescence decay traces under different experimental conditions (i.e., the absence or presence of phosphate buffer with total concentration of C^B and different values of pH and λ_{em}) were recorded, and a complete multi-dimensional decay trace surface was obtained.[24]

The decay traces were analyzed in terms of the decay times, τ_i, and associated pre-exponential factors, p_i (i = 1, 2), by performing global analyses of curves collected at the same pH and C^B but at different λ_{ex} and λ_{em}. The decay times, τ_i, were linked parameters for decay traces recorded with these characteristics, whereas the pre-exponentials were locally adjustable parameters.

In the absence of phosphate buffer, the decay times were biexponential with positive pre-exponential factors. The decay times were also independent of both the emission and excitation wavelengths and the pH. Therefore, ESPT does not occur in the absence of buffer. Global analysis of 66 curves corresponding to C^B = 0 M in the pH range between 4.50 and 10.26 at λ_{ex} = 485 and 530 nm and λ_{em} = 560, 580, and 600 nm provided reliable decay time estimates: τ_1 = 0.990 ± 0.003 ns and τ_2 = 3.78 ± 0.03 ns (χ_g^2 = 1.15). At pH values greater than 8, only τ_2 was present. At these pH values, the reprotonation reaction in the excited state is very slow because of the low concentration of protons and does not compete with the radiative constant. Therefore, this decay time unequivocally defines the value for k_{02}. Nevertheless, the shorter lifetime τ_1 consists of the sum of the excited-state dissociation rate constant, k_{21}, and the radiative constant

of the neutral form, k_{01}. From global analyses of the decay traces, we determined that $k_{02} = 2.64 \times 10^8$ s^{-1} and $k_{01} + k_{21} = 1.08 \times 10^9$ s^{-1}.

To obtain the ESPT rate constants k_{21}^B and k_{12}^B, 366 decay traces were collected in the pH range of 4.00 to 10.26 with different phosphate buffer concentrations (0, 0.15, 0.3, and 0.6 M) at two λ_{ex} (485 and 530 nm) and three λ_{em} (560, 580, and 600 nm) values. The theoretical equations (S8 and S9 in the SI) were fit with the decay times previously determined to obtain the rate constants. Figure 5 shows the decay times determined, along with the fitted curves (χ_g^2=1.18). Global analysis provided all of the rate constants of Scheme 3 (Table 1). During the model fitting, the value of k_{21} was always close to 0 and exhibited a very large associated error. Hence, we considered the spontaneous excited-state deprotonation negligible.

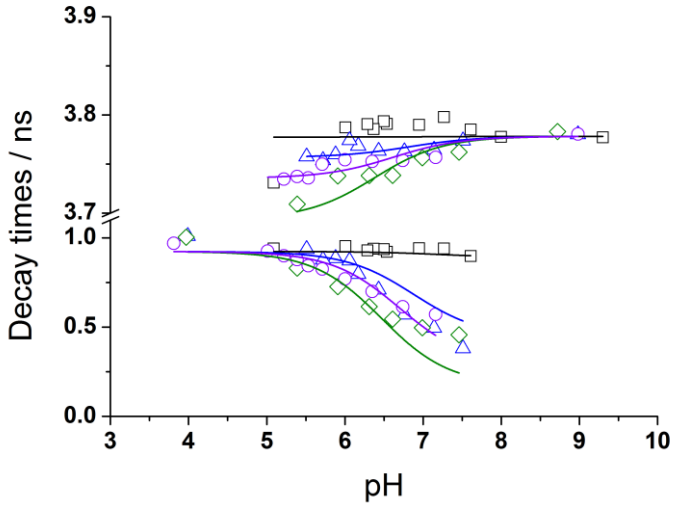

Figure 5. Global fitting (solid lines) of the theoretical equations (S8 to S11 in the SI) to the decay times at different buffer concentrations (0 □, 0.15 Δ, 0.3 O, and 0.6 ◇ M) and pH values. Note the change in scale in the two sections of the ordinate axis.

The relative values of the rate constants k_{21}^{B} and k_{12}^{B} indicate that buffer-mediated deprotonation of the neutral state is two orders of magnitude faster that the excited-state phosphate-assisted protonation of the anion form. This is in perfect agreement with the TRES results, which mainly exhibited excited-state transformation to the anion form. Finally, the rate constants k_{21}^{B} and k_{12}^{B}, along with the known value of $K_a{}^{B}$, can provide the excited-state $pK^{*}_{N\text{-}A}$. Using 7.2 as the $pK_a{}^{B}$, the previously determined rate constants, and equation S10 (SI), we obtained a value of 4.31 for the $pK^{*}_{N\text{-}A}$. This value indicates that **2-Me TM** is a stronger photoacid than the green xanthene derivatives, in which the excited-state p*K** did not vary substantially with respect to the ground-state equilibrium constant.[2, 20, 29-30]

Table 1. Rate constant values for the phosphate-mediated ESPT reaction of **2-Me TM**

Rate Constant	**Value**
k_{01} / s^{-1}	$1.08(\pm0.01)\times10^{9}$
k_{02} / s^{-1}	$2.646(\pm0.009)\times10^{8}$
k_{12}^{B} / M^{-1} s^{-1}	$1.02\ (\pm0.43)\times10^{7}$
k_{21}^{B} / M^{-1} s^{-1}	$7.88\ (\pm0.66)\times10^{9}$

*3.6. Fluorescence imaging microscopy of **2-Me TM** in HeLa cells*

Water solubility and membrane permeability are crucial properties for a fluorescent sensor that functions inside live cells. Some xanthene-based dyes have exhibited good penetration in cells, and they could be used as intracellular sensors.[9-10] In fact, **2-Me TM** βgal was applied to visualize β-galactosidase activity in HEK293 cells.[18] To test the penetration and accumulation of

2-Me TM in the various locations of the cell interior, measurements on live HeLa 229 cells were performed. We monitored the loading (1×10^{-7} M) of the probe in the intracellular compartments. Immediately after the loading, confocal fluorescence imaging was performed. As shown in Figures 6A-D, the intracellular accumulation of **2-Me TM** suggests spontaneous, fast and good membrane penetration without a need for any external molecular assistance. In addition, in contrast with the pattern observed for previous xanthene-based dyes,[9-10] characteristic fluorescence of **2-Me TM** was also observed in the interior of the nucleus. To examine this new accumulation pattern, we measured the intensity profile of the probe in different cellular compartments inside HeLa 229 cells. Figures 6E-H show the profile of the fluorescence intensity signal, which corresponds to the arrows in Figures 6A-D, respectively. In every cell examined, the cytosol and nuclei exhibited a similar intensity of fluorescence. This result suggests that good nuclear membrane penetration of **2-Me TM** allows homogeneous and analogous accumulation of the probe in the cytosol and nuclei. Moreover, the probe exhibited strong accumulation in different cytoplasmic structures. This noticeable signal will permit isolation, differential treatment, and tracking or study of these structures independent of the cytosol/nucleus fluorescence.

Therefore, based on the fluorescence intensity upon excitation of the cells at 530 nm during dye loading, it can be established that **2-Me TM** readily accumulates inside cytoplasmic structures and less effectively but homogeneously accumulates in the cytosol and nucleus.

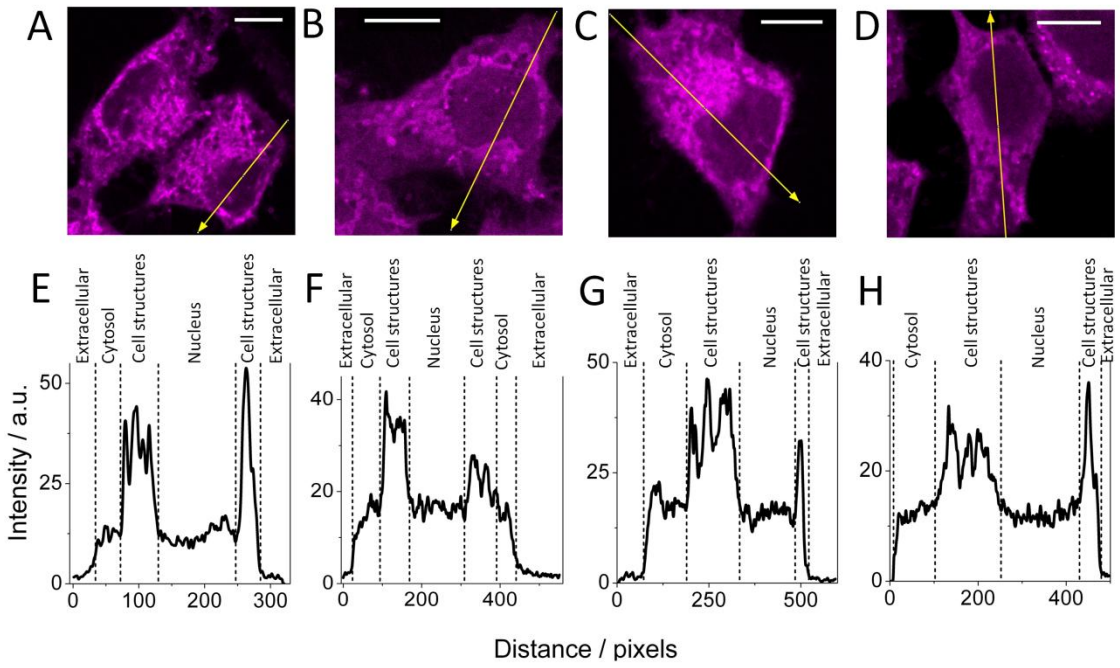

Figure 6. A-D: Illustrative fluorescence images of HeLa 229 cells with **2-Me TM** (10^{-7} M). E-H: Intensity profiles of the arrows from Figures 6A-D, respectively. Scale bars represent 10 μm.

Conclusions

To investigate the use of the new silicon-substituted xanthene derivative **2-Me TM** as a sensor, we have performed a study of the photophysics of the dye. Three absorbing and emitting species have been identified, and the acidity constant of the dye at near-neutral pH was determined using both absorbance and steady-state fluorescence methods. Using steady-state and time-resolved fluorescence experiments, we demonstrated that **2-Me TM** undergoes a phosphate-mediated ESPT reaction and rapidly interconverts between the neutral and anion species. TRES experiments demonstrated a preferred conversion of the neutral form to the anion form, thereby indicating that the buffer-mediated deprotonation of the neutral form is the main process,

whereas buffer-mediated protonation of the anion form is a much slower process. The kinetic parameters determined were consistent with the TRES results, thus indicating a higher rate constant for deprotonation than protonation, which implies a very low value of $pK^*_{N\text{-}A}$. Finally, we used the dye inside cells to examine its future application as a cell sensor. Excitation of the cells at 530 nm indicated that **2-Me TM** accumulates visibly inside cytoplasmic structures and less effectively but homogeneously accumulates in the cytosol and nucleus.

Supporting Information. ^{1}H and ^{13}C NMR data together with a copy of both spectra (figures S1 and S2), analysis of the absorbance vs. pH, analysis of the experimental fluorescence vs. pH, figures S3 to S9, and evaluation of kinetic parameters. This material is available free of charge via the Internet at http://pubs.acs.org.

AUTHOR INFORMATION

Corresponding Author

* To whom correspondence should be addressed: e-mail: jalvarez@ugr.es. Tel. +34 958243831.

Author Contributions

The manuscript was written through contributions of all authors. All authors have given approval to the final version of the manuscript.

ACKNOWLEDGMENT

This research was funded by MINECO (project CTQ2014-56370-R), and MINECO (project CTQ2014-53598).

REFERENCES

1. Diehl, H.; Markuszewski, R., Studies on Fluorescein - VII. The Fluorescence of Fluorescein as a Function Of pH. *Talanta* **1989,** *36*, 416-18.
2. Alvarez-Pez, J. M.; Ballesteros, L.; Talavera, E.; Yguerabide, J., Fluorescein Excited-State Proton Exchange Reactions: Nanosecond Emission Kinetics and Correlation with Steady-State Fluorescence Intensity. *J. Phys. Chem. A* **2001,** *105*, 6320-6332.
3. Yguerabide, J.; Talavera, E.; Alvarez, J. M.; Quintero, B., Steady-State Fluorescence Method for Evaluating Excited State Proton Reactions: Application to Fluorescein. *Photochem. Photobiol.* **1994,** *60*, 435-41.
4. Paradiso, A. M.; Tsien, R. Y.; Machen, T. E., Na+-H+ exchange in gastric glands as measured with a cytoplasmic-trapped, fluorescent pH indicator. *Proc. Natl. Acad. Sci. U. S. A.* **1984,** *81*, 7436-40.
5. Rink, T. J.; Tsien, R. Y.; Pozzan, T., Cytoplasmic pH and Free Mg^{2+} in Lymphocytes. *J. Cell Biol.* **1982,** *95*, 189-196.
6. Boens, N.; Qin, W.; Basaric, N.; Orte, A.; Talavera, E. M.; Alvarez-Pez, J. M., Photophysics of the Fluorescent pH Indicator BCECF. *J. Phys. Chem. A* **2006,** *110*, 9334-9343.
7. Urano, Y.; Kamiya, M.; Kanda, K.; Ueno, T.; Hirose, K.; Nagano, T., Evolution of Fluorescein as a Platform for Finely Tunable Fluorescence Probes. *J. Am. Chem. Soc.* **2005,** *127*, 4888-4894.
8. Martinez-Peragon, A.; Miguel, D.; Jurado, R.; Justicia, J.; Alvarez-Pez, J. M.; Cuerva, J. M.; Crovetto, L., Synthesis and Photophysics of a New Family of Fluorescent 9-Alkyl-Substituted Xanthenones. *Chem. - Eur. J.* **2014,** *20*, 447-455.
9. Martinez-Peragon, A.; Miguel, D.; Orte, A.; Mota, A. J.; Ruedas-Rama, M. J.; Justicia, J.; Alvarez-Pez, J. M.; Cuerva, J. M.; Crovetto, L., Rational Design of a New Fluorescent 'ON/OFF' Xanthene Dye for Phosphate Detection in Live Cells. *Org. Biomol. Chem.* **2014,** *12*, 6432-6439.
10. Paredes, J. M.; Giron, M. D.; Ruedas-Rama, M. J.; Orte, A.; Crovetto, L.; Talavera, E. M.; Salto, R.; Alvarez-Pez, J. M., Real-Time Phosphate Sensing in Living Cells using Fluorescence Lifetime Imaging Microscopy (FLIM). *J. Phys. Chem. B* **2013,** *117*, 8143-8149.
11. Fu, M.; Xiao, Y.; Qian, X.; Zhao, D.; Xu., Y., A Design Concept of Long-Wavelength Fluorescent Analogs of Rhodamine Dyes: Replacement of Oxygen With Silicon Atom. *Chem. Commun.* **2008**, 1780-1782.
12. Koide, Y.; Urano, Y.; Hanaoka, K.; Terai, T.; Nagano, T., Evolution of Group 14 Rhodamines as Platforms for Near-Infrared Fluorescence Probes Utilizing Photoinduced Electron Transfer. *ACS Chem. Biol.* **2011,** *6*, 600-608.
13. Pastierik, T.; Sebej, P.; Medalova, J.; Stacko, P.; Klan, P., Near-Infrared Fluorescent 9-Phenylethynylpyronin Analogues for Bioimaging. *J. Org. Chem.* **2014,** *79*, 3374-3382.
14. Egawa, T.; Hirabayashi, K.; Koide, Y.; Kobayashi, C.; Takahashi, N.; Mineno, T.; Terai, T.; Ueno, T.; Komatsu, T.; Ikegaya, Y.*, et al.*, Red Fluorescent Probe for Monitoring the Dynamics of Cytoplasmic Calcium Ions. *Angew. Chem., Int. Ed.* **2013,** *52*, 3874-3877.
15. Hirabayashi, K.; Hanaoka, K.; Takayanagi, T.; Toki, Y.; Egawa, T.; Kamiya, M.; Komatsu, T.; Ueno, T.; Terai, T.; Yoshida, K.*, et al.*, Analysis of Chemical Equilibrium of Silicon-Substituted Fluorescein and Its Application to Develop a Scaffold for Red Fluorescent Probes. *Anal. Chem.* **2015,** *87*, 9061-9069.

16. Koide, Y.; Urano, Y.; Hanaoka, K.; Piao, W.; Kusakabe, M.; Saito, N.; Terai, T.; Okabe, T.; Nagano, T., Development of NIR Fluorescent Dyes Based on Si–rhodamine for in Vivo Imaging. *J. Am. Chem. Soc.* **2012,** *134*, 5029-5031.
17. Kushida, Y.; Nagano, T.; Hanaoka, K., Silicon-Substituted Xanthene Dyes and Their Applications in Bioimaging. *Analyst* **2015,** *140*, 685-695.
18. Egawa, T.; Koide, Y.; Hanaoka, K.; Komatsu, T.; Terai, T.; Nagano, T., Development of a Fluorescein Analogue, Tokyo Magenta, as a Novel Scaffold for Fluorescence Probes in Red Region. *Chem.Commun.* **2011,** *47*, 4162-4164.
19. Orte, A.; Bermejo, R.; Talavera, E. M.; Crovetto, L.; Alvarez-Pez, J. M., 2',7'-difluorofluorescein Excited-State Proton Reactions: Correlation between Time-Resolved Emission and Steady-State Fluorescence Intensity. *J. Phys. Chem. A* **2005,** *109*, 2840-2846.
20. Orte, A.; Crovetto, L.; Talavera, E. M.; Boens, N.; Alvarez-Pez, J. M., Absorption and Emission Study of 2 ',7 '-difluorofluorescein and Its Excited-State Buffer-Mediated Proton Exchange Reactions. *J. Phys. Chem. A* **2005,** *109*, 734-747.
21. O'Connor, D. V.; Phillips, D., *Time-correlated single photon counting*. Academic Press: 1984.
22. Badea, M. G.; Brand, L., [17] Time-resolved fluorescence measurements. In *Methods Enzymol.*, C.H.W. Hirs, S. N. T., Ed. Academic Press: 1979; Vol. Volume 61, pp 378-425.
23. Janssens, L. D.; Boens, N.; Ameloot, M.; De Schryver, F. C., A Systematic Study of the Global Analysis of Multiexponential Fluorescence Decay Surfaces Using Reference Convolution. *J. Phys. Chem.* **1990,** *94*, 3564-3576.
24. Boens, N.; Basarić, N.; Novikov, E.; Crovetto, L.; Orte, A.; Talavera, E. M.; Alvarez-Pez, J. M., Identifiability of the Model of the Intermolecular Excited-State Proton Exchange Reaction in the Presence of pH Buffer. *J. Phys. Chem. A* **2004,** *108*, 8180-8189.
25. Best, Q. A.; Sattenapally, N.; Dyer, D. J.; Scott, C. N.; McCarroll, M. E., pH-Dependent Si-Fluorescein Hypochlorous Acid Fluorescent Probe: Spirocycle Ring-Opening and Excess Hypochlorous Acid-Induced Chlorination. *J. Am. Chem. Soc.* **2013,** *135*, 13365-13370.
26. Lakowicz, J. R., *Principles of Fluorescence Spectroscopy*. 3rd ed.; Springer: 2006.
27. Schindelin, J.; Arganda-Carreras, I.; Frise, E.; Kaynig, V.; Longair, M.; Pietzsch, T.; Preibisch, S.; Rueden, C.; Saalfeld, S.; Schmid, B.*, et al.*, Fiji: an Open-Source Platform for Biological-Image Analysis. *Nat. Meth.* **2012,** *9*, 676-682.
28. Crovetto, L.; Paredes, J. M.; Rios, R.; Talavera, E. M.; Alvarez-Pez, J. M., Photophysics of a Xanthenic Derivative Dye Useful as an 'On/Off' Fluorescence Probe. *J. Phys. Chem. A* **2007,** *111*, 13311-13320.
29. Paredes, J. M.; Crovetto, L.; Rios, R.; Orte, A.; Alvarez-Pez, J. M.; Talavera, E. M., Tuned Lifetime, at the Ensemble and Single Molecule Level, of a Xanthenic Fluorescent Dye by Means of a Buffer-Mediated Excited-State Proton Exchange Reaction. *Phys. Chem. Chem. Phys.* **2009,** *11*, 5400-5407.
30. Paredes, J. M.; Orte, A.; Crovetto, L.; Alvarez-Pez, J. M.; Rios, R.; Ruedas-Rama, M. J.; Talavera, E. M., Similarity between the Kinetic Parameters of the Buffer-Mediated Proton Exchange Reaction of a Xanthenic Derivative in its Ground- and Excited-State. *Phys. Chem. Chem. Phys.* **2010,** *12*, 323-327.
31. Crovetto, L.; Orte, A.; Talavera, E. M.; Alvarez-Pez, J. M.; Cotlet, M.; Thielemans, J.; De Schryver, F. C.; Boens, N., Global Compartmental Analysis of the Excited-State Reaction between Fluorescein and (+/-)-N-Acetyl Aspartic Acid. *J. Phys. Chem. B* **2004,** *108*, 6082-6092.

Supporting Information for

Photophysics of a Live-Cell-Marker, Red Silicon-Substituted Xanthene Dye.

*Luis Crovetto,[1] Angel Orte,[1] Jose M. Paredes,[1] Sandra Resa,[2] Javier Valverde,[1] Fabio Castello,[1] Delia Miguel,[2] Juan M. Cuerva,[2] Eva M. Talavera,[1] and Jose M. Alvarez-Pez[1,]**

[1] Department of Physical Chemistry, Faculty of Pharmacy, University of Granada, Cartuja Campus, 18071 Granada, Spain.

[2] Department of Organic Chemistry, Faculty of Sciences, University of Granada, C. U. Fuentenueva s/n, 18071 Granada, Spain.

*Author to whom correspondence should be addressed.
Tel.: + 34-958-243831; fax: + 34-958-244090; e-mail: **jalvarez@ugr.es**

TABLE OF CONTENTS

^{1}H NMR and ^{13}C NMR data of 2-Me TM:

^{1}H NMR (500 MHz, CD_3OD)δ= 7.45 – 7.33 (m, 3H), 7.11 (d, *J* = 7.3 Hz, 1H), 7.04 (d, *J* = 2.4 Hz, 2H), 6.94 (d, *J* = 9.5 Hz, 2H), 6.45 (dd, *J* = 9.5, 2.3 Hz, 2H), 2.05 (s, 3H), 0.51 (s, 3H), 0.49 (s, 3H).

^{13}C NMR (126 MHz, CD_3OD) δ = 161.5 (C), 146.9 (C), 141.0 (C), 140.6 (CH), 137.1 (CH), 131.3 (CH), 130.9 (C), 130.0 (C), 130.3 (CH), 129.7 (CH), 126.9 (CH), 122.8 (C), 19.5 (CH_3), -1.3 (CH_3), -1.6 (CH_3).

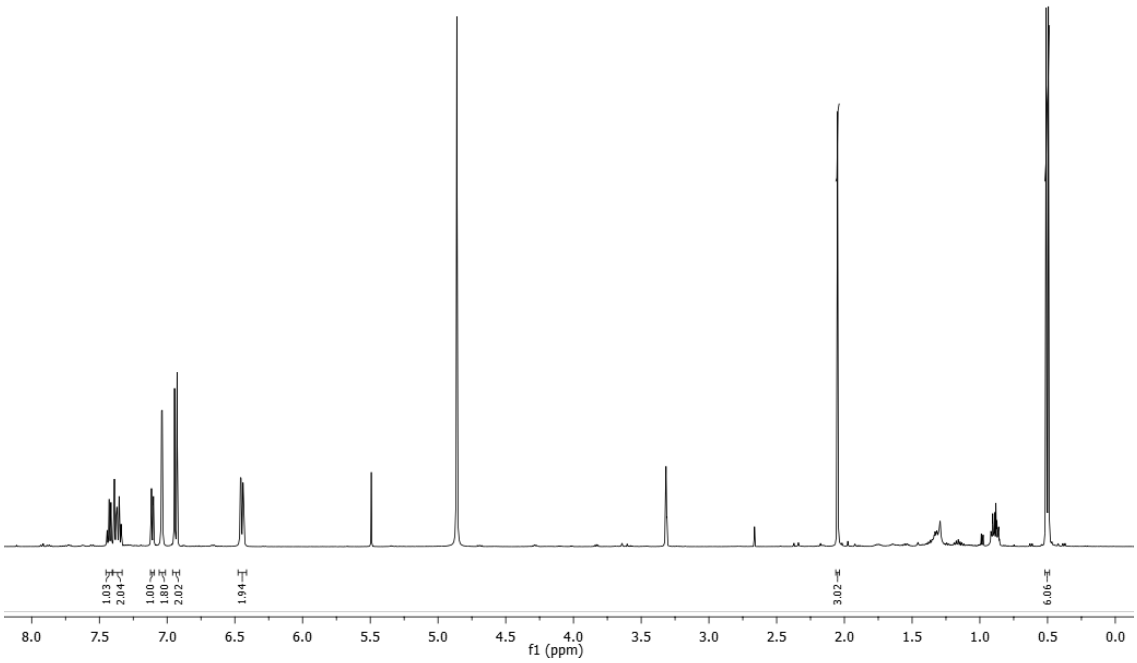

Figure S1. ^{1}H-NMR spectrum of 2-Me TM

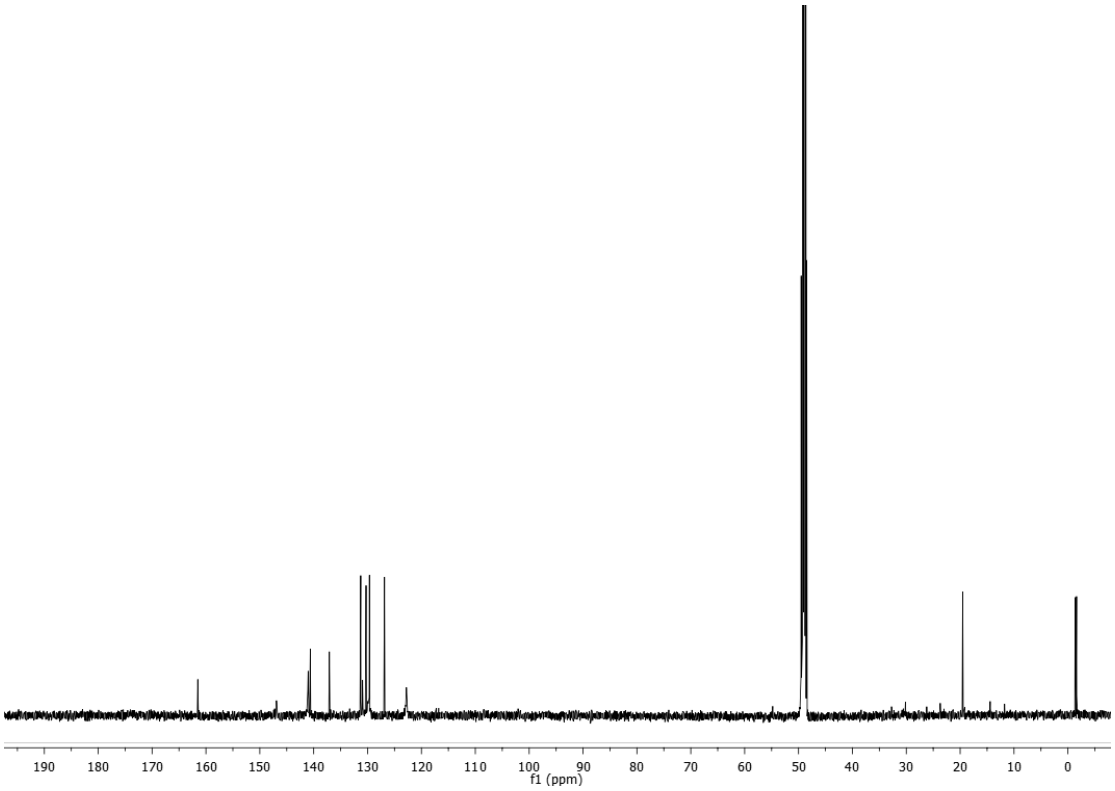

Figure S2. ^{13}C-NMR spectrum of 2-Me TM

Analysis of the experimental absorbance versus pH used to determine the ground-state equilibrium of 2-Me TM

If a neutral/anion system follows Beer's law, at any wavelength (λ_{abs}) and pH, the absorbance (A) is given by the expression

$$A(\mathrm{p}H, \lambda_{abs}) = C^{TM}\left(\sum_i \alpha_i(\mathrm{p}H, \mathrm{p}K_{N-A})\varepsilon_i(\lambda_{abs})\right)d\,, \qquad \text{(S1)}$$

where C^{TM} is the total concentration of **2-Me TM**, d is the optical path length, $\varepsilon_i(\lambda_{abs})$ is the wavelength-dependent molar absorption coefficient of the ith prototropic form of **2-Me TM**, and $\alpha_i(\mathrm{p}H, \mathrm{p}K_{\mathrm{N\text{-}A}})$ is the fraction of **2-Me TM** in the ith prototropic form, which depends on both pH and p$K_{\mathrm{N\text{-}A}}$.

$$\alpha_N = \frac{[H^+]}{[H^+] + K_{N-A}} \qquad \text{(S2)}$$

$$\alpha_A = \frac{K_{N-A}}{[H^+] + K_{N-A}} \qquad \text{(S3)}$$

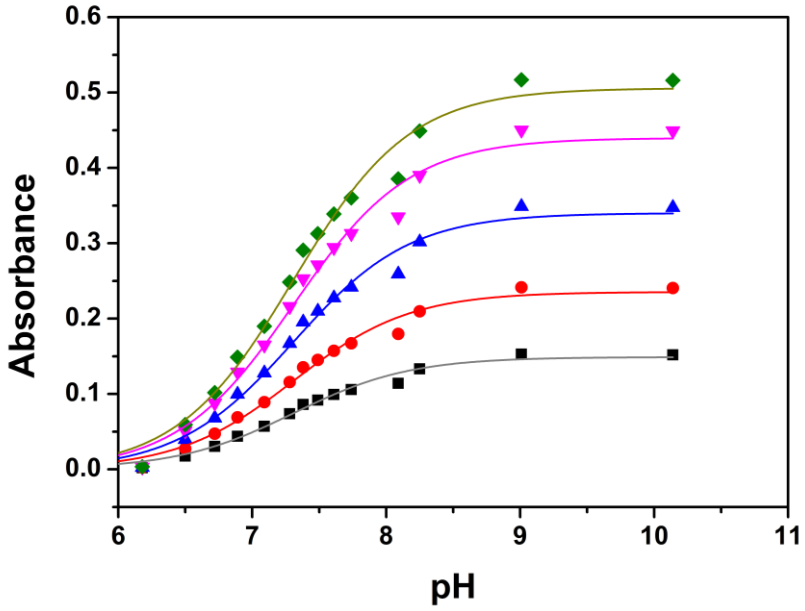

Figure S3. Curves generated by fitting the individual $A(\lambda_{abs})$ versus pH data.

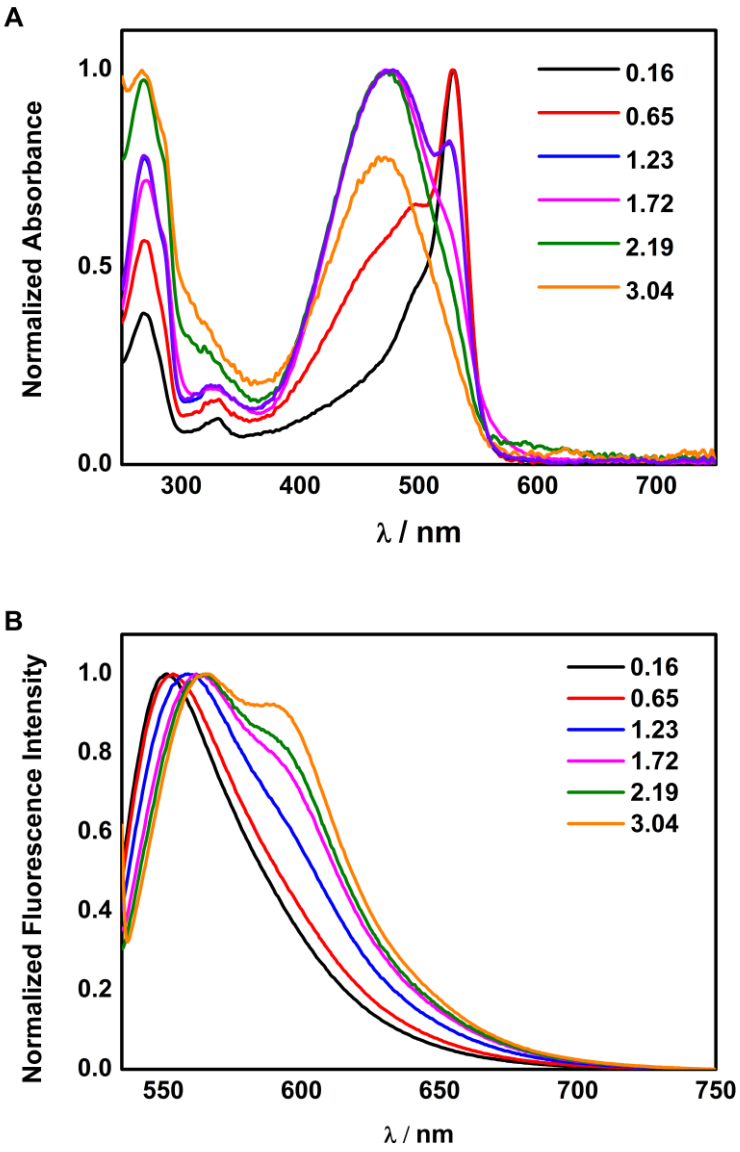

Figure S4. (A) Normalized absorbance spectra and (B) their corresponding normalized emission spectra (λ_{ex} 530 nm) at different acidic pH values.

Analysis of the experimental fluorescence versus pH used to determine the ground-state equilibrium of 2-Me TM

The total fluorescence signal $F(\lambda_{ex}, \lambda_{em}, [H^+])$ at proton concentration $[H^+]$ due to excitation at λ_{ex} and observed at emission wavelength λ_{em} can be expressed as

$$F\left(\lambda_{ex},\lambda_{em},[H^+]\right)=\frac{F_{min}[H^+]+F_{max}K_a}{K_a+[H^+]}, \qquad \text{(S4)}$$

where F_{min} indicates the fluorescence signal of the neutral form of the dye and F_{max} denotes the fluorescence signal of the anion form of **2-Me TM**. Fitting eq. S4 to the fluorescence data $F(\lambda_{ex}, \lambda_{em}, [H^+])$ as a function of $[H^+]$ yields values for K_a, F_{min}, and F_{max}.

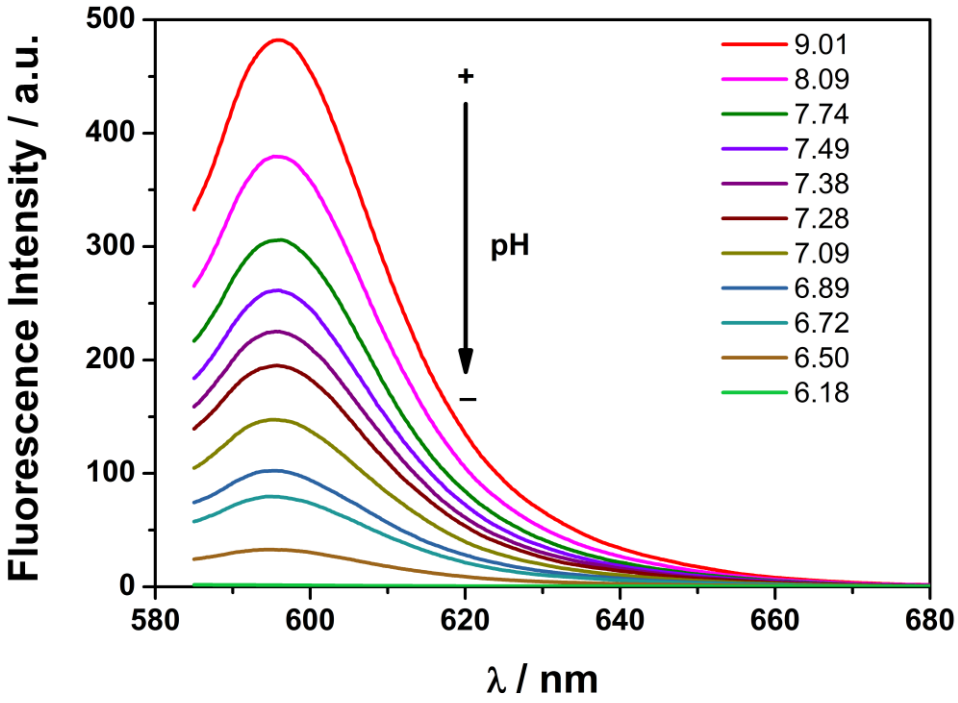

Figure S5. Steady-state emission spectra at λ_{ex}= 580 nm for 1×10^{-6} M **2-Me TM** aqueous solutions in a pH range between 6.18 and 9.00. The arrow indicates a decrease in pH value.

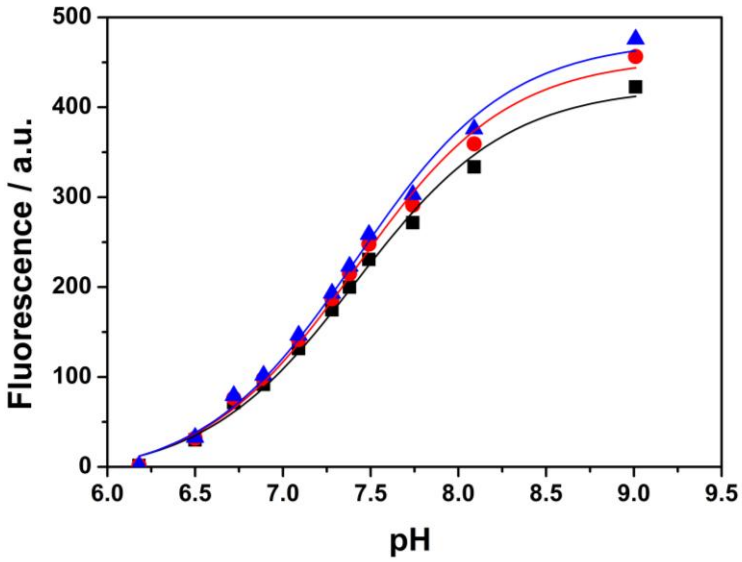

Figure S6. Curves generated by fitting the steady-state fluorescence emission data (λ_{ex}= 580 nm, λ_{em}= 590 nm, black; 592 nm, red; 594 nm, blue) from 1× 10^{-6} M **2-Me TM** aqueous solutions in the pH range between 6.18 and 9.00.

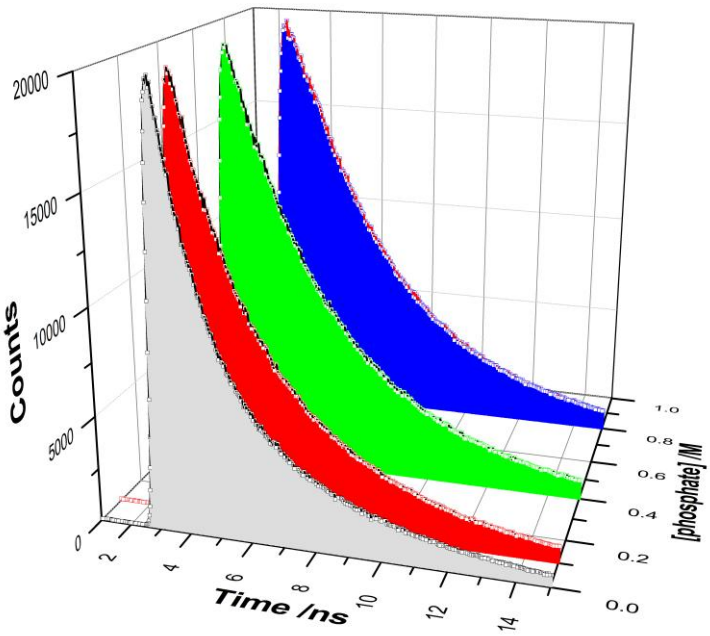

Figure S7. Fluorescence decay traces for an aqueous solution of 5×10^{-5} M **2-Me TM** at pH 6.10 with different phosphate buffer concentrations: 0.005 (black), 0.1 (red), 0.4 (green), and 0.8 M (blue).

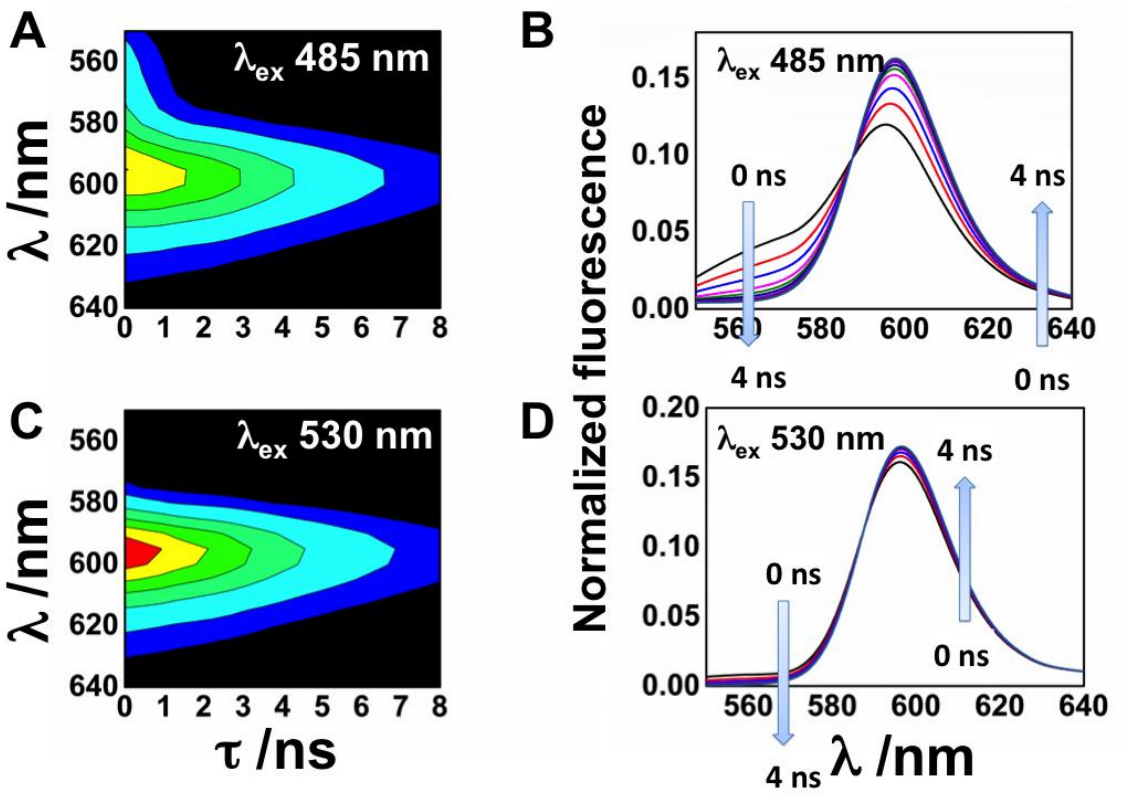

Figure S8. Contours of fluorescence intensity of **2-Me TM** after a δ-pulse excitation as a function of time and λ_{em} in 0.7 M phosphate buffer at pH 6.61 (A: λ_{ex} 485 nm; C: λ_{ex} 530 nm). The corresponding normalized emission spectra at different times after the excitation pulse are shown (B: λ_{ex} 485 nm; D: λ_{ex} 530 nm).

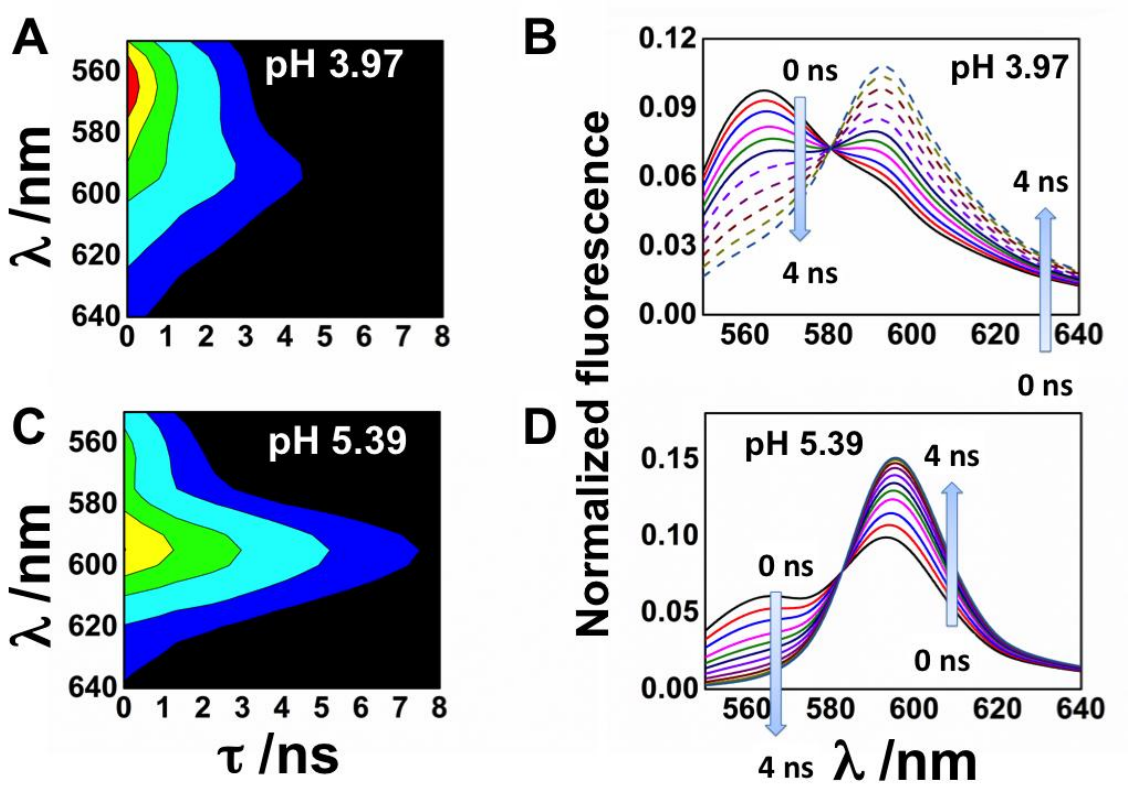

Figure S9. Contours of fluorescence intensity of **2-Me TM** after a 485-nm δ-pulse excitation as a function of time and λ_{em} in 0.7 M phosphate buffer at pH 3.97 (A) and 5.39 (C). The corresponding normalized emission spectra at different times after the excitation pulse are shown (B: pH 3.97; D: pH 5.39).

Evaluation of kinetic parameters from the lifetimes at high phosphate buffer concentrations

For scheme 2, the solution of the coupled differential rate equations consists of well-known biexponential expressions:[S1]

$$[2*] = \beta_{2S}\, e^{\gamma_S t} + \beta_{2L}\, e^{\gamma_L t} \qquad \text{(S5)}$$

$$[1*] = \beta_{1S}\, e^{\gamma_S t} + \beta_{1L}\, e^{\gamma_L t}, \qquad \text{(S6)}$$

where

$$\gamma_{1,2} = \frac{-(a+c) \mp \sqrt{(c-a)^2 + 4bd}}{2}; \qquad \text{(S7)}$$

$a=k_{01}+ k_{21}+ k^B_{21}[R]$; $b=k_{12}[H^+]+ k^B_{12}[RH]$; $c=k_{02} + k_{12}[H^+]+ k^B_{12}[RH]$; and $d=k_{21}+ k^B_{21}[R]$. $[R]$ and $[RH]$ are related to the total buffer concentration, C^B=[R]+$[RH]$, by the expressions $[RH] = C^B\,[H^+]/([H^+]+ K_a{}^B)$ and $[R] = C^B\,K_a{}^B/([H^+]+ K_a{}^B)$, where $K_a{}^B$ is the dissociation constant for the reversible reaction $RH \leftrightarrow R + H^+$.

The γ factors are related to the lifetimes τ_1 and τ_2 by the expression

$$\tau_{1,2} = -\frac{1}{\gamma_{1,2}}. \qquad \text{(S8)}$$

The rate constants k^B_{21} and k^B_{12}, along with the known value of $K_a{}^B$, can provide the excited-state p$K^*_{n\text{-}a}$ according to the equation

$$pK^*_{n-a} = \log\left(k^B_{12}\right) - \log\left(k^B_{21}\right) + pK^B_a. \qquad \text{(S9)}$$

REFERENCES

[S1] Alvarez-Pez, J. M.; Ballesteros, L.; Talavera, E. M.; Yguerabide, J. *J. Phys. Chem. A* **2001**, *105*, 6320.